Spontaneous Coherent Phase Transition of Polaritons in CdTe Microcavities

Maxime Richard, Jacek Kasprzak, Robert Romestain, Régis André, and Le Si Dang

CEA-CNRS-UJF group "Nanophysique et semiconducteurs," Laboratoire de Spectrométrie Physique (CNRS UMR5588), Université J. Fourier–Grenoble, BP87, 38402 St Martin d'Hères, France

(Received 6 May 2004; revised manuscript received 27 August 2004; published 12 May 2005)

We report on evidence for polariton condensation out of a reservoir of incoherent polaritons. Polariton population and first-order coherence are investigated by spectroscopic imaging of the far-field emission of a CdTe-based microcavity under nonresonant pumping. With increasing pumping power, stimulated emission with thresholdlike behavior and spectral narrowing is observed in the strong exciton-photon coupling regime. We show that it comes from a narrow ring in k space, exhibiting enhanced spatial and angular coherence at the stimulation onset.

DOI: 10.1103/PhysRevLett.94.187401 PACS numbers: 78.45.+h, 03.75.Nt, 42.50.−p, 71.36.+c

Bose-Einstein condensation (BEC) is the unique feature of bosons to collapse into the lowest quantum state below a critical temperature [1]. It was predicted in the 1920s and demonstrated in 1995 with a gas of atoms cooled down to the nK range [2]. The quest for BEC in solid state systems started with excitons in bulk semiconductors [3–5], then with excitons in coupled quantum wells [6–9], and recently with microcavity polaritons (polaritons) [10–17]. For these bosons, the critical temperature would be in the K range because of their small masses, particularly in the case of polaritons.

Polaritons are two-dimensional eigenstates of semiconductor microcavities with embedded quantum wells [18–20]. They result from the strong coupling between photon modes confined in the microcavity and excitons confined in quantum wells. Because of their mixed photon-exciton nature, they acquire some of the photon features which differ markedly from those of excitons. Of interest for BEC is the polariton mass which is 4 orders of magnitude smaller as compared to that of excitons. Thus, in addition to the expected higher critical temperature, condensation should occur at much lower densities for polaritons than for excitons. This is an important issue since polaritons and excitons are composite bosons, rather fragile with respect to Coulomb screening. Unfortunately the polariton lifetime is typically in the picosecond time scale, which is too short to allow thermalization with the lattice through interaction with phonons, and possibly to achieve BEC.

On the other hand, collective and coherence effects of polaritons have been reported under high pumping conditions. In CdTe-based microcavities, stimulated emission and spectral narrowing have been observed for the polariton ground state under nonresonant pumping [14,15]. In GaAs-based microcavities, macroscopic coherent occupation of the polariton ground state has been realized in parametric scattering experiments by pumping resonantly into the lower polariton branch. This results in strong modifications of the polariton dispersion which have been interpreted in terms of coherent scatterings within polariton condensates [21]. Recently polariton emission in a GaAs-based microcavity and the related second-order coherence function have been measured under resonant pumping into polariton states with large in-plane wave vectors, at less than 10 meV above the polariton ground state [16]. Results are found to be consistent with the formation of a polariton condensate. To our knowledge no clear-cut evidence of polariton condensation and induced coherence under a strictly nonresonant pumping condition has been reported so far in any microcavity system.

In the present work, we report on the spontaneous formation of a fully coherent phase of polaritons out of a reservoir of incoherent polaritons. Evidence for the first-order coherence was provided by spectroscopic imaging measurements when pumping 100 meV above the polariton ground state. Experiments were performed at 5 K using a CdTe-based microcavity, with the exciton energy resonant with the cavity mode energy. The exciton binding energy in CdTe quantum wells (QWs) is larger than in GaAs QWs, typically 25 meV as compared to 10 meV. Thus, with its higher exciton screening density, about 5×10^{11} cm^{-2} [14], CdTe is well suited for high excitation studies. The far-field emission of the microcavity was measured as a function of pumping power. It was found that dramatic changes were induced above a threshold power. First, polariton emission intensity increased with an exponential rate. Second, polaritons condensed in a set of degenerate quantum states forming a ring in k space. Third, marked speckles appeared in the far-field emission as well as strong interference effects in far-field emission patterns generated by a Billet interferometer. The combination of these observations demonstrates the spontaneous buildup of polaritons in a macroscopic coherent phase.

The microcavity sample consists of 16 CdTe/CdMgTe QWs embedded in a 2λ CdMgTe microcavity with CdMnTe/CdMgTe Bragg mirrors. It was grown by molecular beam epitaxy, and details on the sample growth can be found in [15]. The microcavity exhibits a vacuum Rabi splitting of 26 meV. A Ti:sapphire laser delivering 100 fs long pulses at 80 MHz was used to excite electron-hole

pairs in CdTe QWs. The laser energy was set at about 1.77 eV to avoid any direct absorption into the lower polariton branch at about 1.67 eV. Photoluminescence (PL) was measured with a typical integration time of 100 ms. Thus PL measured above stimulation threshold is a superimposition of stimulated PL, emitted typically within 10 ps after the excitation pulse, and spontaneous PL which decays over a few hundreds of ps [22]. Note that this could result in an underestimate of polariton coherence in the stimulation regime as is discussed later.

To have access to the far-field emission of the microcavity, we used the experimental setup sketched in Fig. 1. The laser beam was focused to a 3 μm diameter spot on the sample by a microscope objective (focal length $f_1 = 9$ mm). The PL was collected through the same objective lens, and an achromatic lens ($f_2 = 180$ mm) was used to form the image of the Fourier plane onto either a CCD camera or the entrance slit of a 1 m focal length monochromator. Note that each point in the Fourier plane is the superimposition of photon fields emitted by the source along a given direction (θ, ϕ), where θ is the emission angle with respect to the normal to the microcavity plane and ϕ is the azimuth angle. Thus far-field emission of an extended source but also its spatial coherence can be conveniently examined by imaging the Fourier plane. With the CCD camera, one gets directly images (θ, ϕ) of the spectrally integrated far-field emission as shown in Figs. 2(a) and 2(d). Accessible angles θ were limited by the numerical aperture of the microscope objective to the range $\pm 23.6°$. For planar microcavities, photons emitted at angle θ are due to the recombination of polaritons with the in-plane wave vector $k_\parallel = k_0 \sin(\theta)$ (where k_0 is the wave number of the emitted light). By using a monochromator in the Fourier plane image (see Fig. 1), one obtains a direct image (θ, E) of the polariton dispersion curve $E(\theta)$ as shown in Figs. 2(b) and 2(e). This allows probing the population distribution of polaritons along the lower polariton branch, for example.

This setup can be easily transformed into a Billet interferometer by replacing the achromatic lens by two half lenses. Then the far-field emission of the microcavity is split into two parts, one part corresponding to the half plane $\phi = [0, \pi]$ of azimuth angle of emission and the other part corresponding to the half plane $\phi = [\pi, 2\pi]$. By moving symmetrically apart the half lenses along a direction perpendicular to the optical axis, one can vary the spatial overlap between the two half far-field emissions in the Fourier plane image. This allows one to observe directly interference between two polariton states $k_\parallel + \Delta k_\parallel/2$ and $k_\parallel - \Delta k_\parallel/2$. The magnitude and direction of $\Delta k_\parallel$ depend on the displacements of the two half lenses. The resulting interference patterns in the Fourier plane image can be analyzed spectrally with a monochromator, yielding 2D images (θ, E) as displayed in Figs. 3(a) and 3(b). It is important to note that, by contrast to the first experimental setup with a single imaging lens, one obtains here interferences between polariton states of different wave vectors $k_\parallel$, that is, with different emission angles (θ, ϕ).

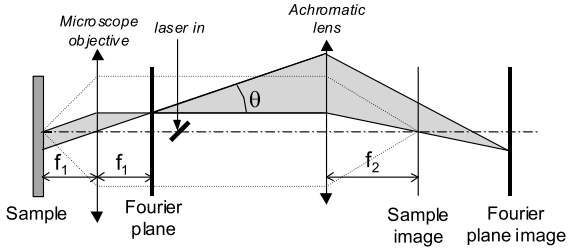

FIG. 1. Real-space and k-space imaging setup: the ray path for real-space imaging is represented by the dashed line, while the ray path for k-space imaging is represented as a gray surface for the emission cone of angle θ.

We first discuss far-field emission results shown in Fig. 2. Figures 2(a) and 2(d) are 2D images (θ, ϕ) of the far-field emission below and above the stimulation threshold, respectively. For low pumping, polariton emission is ringlike, covering a broad range of angle $\theta = 7°$–$20°$ [Fig. 2(a)], and with a rather uniform intensity distribution with respect to the azimuth angle ϕ [Fig. 2(c)]. This corresponds to the well-known bottleneck effect [23–25]. This latter is also visible in the image (θ, E) in Fig. 2(b), which shows polariton PL along the familiar parabolic dispersion curve. It can be seen that strongest PL was emitted by polaritons at angle $\theta \sim 17°$.

Increasing pumping power results in an unusual redistribution of the polariton population. Polaritons at bottleneck do not relax towards the $k_\parallel = 0$ state as predicted in the polariton-polariton scattering model of Porras *et al.* [11] and as experimentally observed [24]. Instead they "condensed" into $k_\parallel \neq 0$ states [Fig. 2(e)], leading to a well defined ring emission at angle $\theta \sim 17°$ [Fig. 2(d)] and an exponential increase of intensity with pumping power [26]. The emission line became as narrow as 0.2 meV, that is, 1 order of magnitude narrower than the cavity mode. It is important to note that the stimulated emission energy was more than 10 meV below the bare cavity mode and quantum well exciton. This clearly indicates that the microcavity was still in the strong exciton-photon coupling regime.

Changing the exciton-photon detuning in the range $[+5$ meV, -20 meV$]$ slightly changes the energy of the stimulated emission with respect to the bottom of the dispersion curve, but not the ringlike feature. Above threshold, polaritons simultaneously present in the ring are estimated to be between 10 to 40 polaritons per quantum state. The observed spectral narrowing shows that the polariton condensate decays coherently with a characteristic time much longer than the individual polariton lifetime (typically 1 ps). In Fig. 2(e) one can also observe a weak luminescence line joining the two stimulated polariton states of opposite wave vectors selected by the mono-

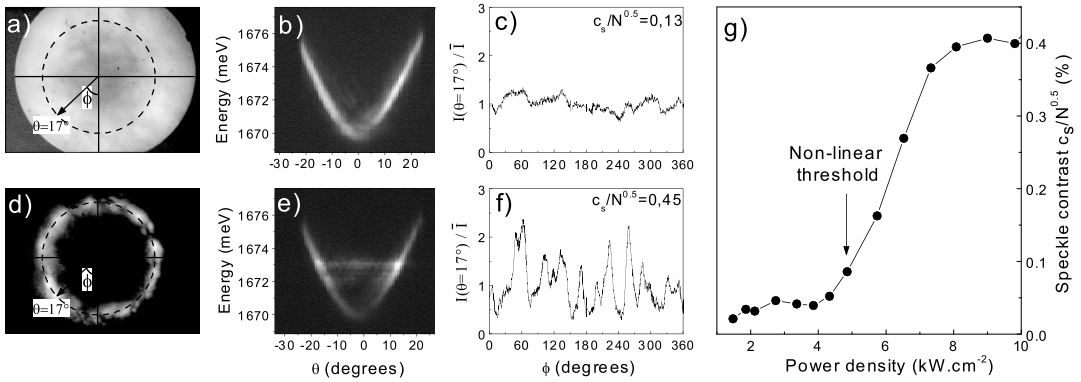

FIG. 2. Far-field emission for two excitation powers: first row and second row of images are obtained below and above the stimulation threshold, respectively. (a) and (d) display the far-field emission in the (θ, ϕ) Fourier plane with a linear scale of gray. The dotted circle plots the cone of angle $\theta = 17°$ where the stimulated emission occurs. (b) and (e) display the emission measured directly in the (θ, E) plane on a logarithmic scale of gray. (c) and (f) display the intensity profile along the azimuth angle ϕ for $\theta = 17°$. (g) displays the evolution of the spatial degree of coherence c_s versus the excitation power. The threshold for increased coherence is the same as that for the stimulated emission.

chromator slit. This luminescence arises from the finite angular width of the stimulated polariton emission from the ring. These photons will be useful for the angular coherence measurement presented below.

Another feature of the stimulated ring emission is the strong intensity variation along the azimuth angle ϕ [Fig. 2(f)]. It bears strong similarities with a recent PL study of GaAs microcavity using resonant pumping [27]. It was shown that direct pumping into the lower polariton branch at $k_{\|} > 0$ results in ringlike emission of polaritons with marked speckles. This observation has been interpreted as being due to elastic scatterings within the population of coherent polaritons photocreated by the resonant pump. In this work, speckles were observed for nonresonant pumping and only in the stimulation regime (compare PL intensity profiles in Figs. 2(c) and 2(f)].

Speckles in the Fourier plane characterized in Fig. 2(f) are closely related to the spatial coherence of the emitting source (and to disorder), since each point in the Fourier plane corresponds to polaritons with a given wave vector $k_{\|}$ emitted by the whole source surface. To get a quantitative evaluation of the coherence, one can follow the statistical analysis of Langbein *et al.* [28], who show that the spatial coherence c_s of the source verifies $c_s = \sqrt{N}\sigma_I/\bar{I}$, where N is the number of independent scatterers involved in the observed speckles, $\bar{I}$ is the mean value of the PL intensity profile along the azimuth ϕ, and σ_I is its standard deviation. Results of such an analysis for different pumping powers are displayed in Fig. 2(g). A strong increase in the spatial coherence of the source is clearly observed with increased pumping. As could be expected, it coincides with the onset of stimulated emission and spectral narrowing, confirming the stimulated buildup of polariton population in a well defined quantum state.

Angular polariton coherence was also investigated with the Billet interferometer setup. Figure 3(a) is a 2D $(k_{\|} \pm \Delta k_{\|}/2, E)$ image displaying the two half parts of the polariton far-field emission in the weak excitation regime. In this regime, polariton emission is distributed over a wide range of wave vectors $k_{\|}$. The monochromator selects the interference between two degenerate polariton states of opposite wave vectors $k_{\|} = \pm\Delta k_{\|}/2$. For example, Fig. 3(a) exhibits the interference between $k_{\|} = \pm 0.45\ \mu\mathrm{m}^{-1}$ polariton states.

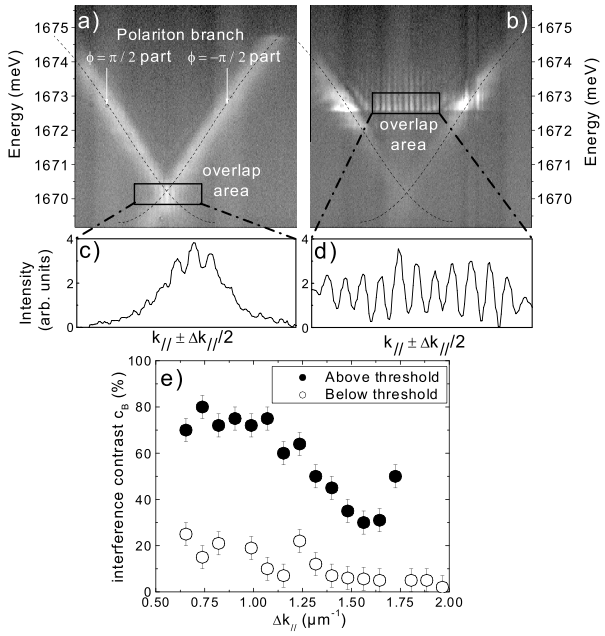

FIG. 3. (a),(b) Images obtained with the Billet interferometer for $\Delta k_{\|} = 0.9\ \mu\mathrm{m}^{-1}$ below and above stimulation threshold, respectively. The gray scale is linear. (c),(d) Profiles of the interference pattern area of the above images. (e) Contrast of interference versus displacement $\Delta k_{\|}$.

At the nonlinear threshold, we have seen that a weak straight line of luminescence constituted by photons from the whole stimulated ring appears in the (θ, E) plane. With the Billet interferometer, this luminescence line overlaps with itself over a wide range of wave vector, resulting in remarkably contrasted interference patterns [see Figs. 3(b) and 3(d) obtained for the same $\Delta k_{\|}$ as Figs. 3(a) and 3(c)].

To have a quantitative analysis of the Billet interferometer measurements, we define the interference contrast by $c_B = (I_{\max} - I_{\min})/(I_{\max} + I_{\min})$, where $I_{\max}$ and $I_{\min}$ are the maximum and minimum PL intensities along interference profiles. Results are given in Fig. 3(e) for various displacements $\Delta k_{\|}$. It can be seen that in the stimulation regime c_B can be as high as 75% in the range $\delta k_{\|} = 0.5$–$1.1\ \mu\mathrm{m}^{-1}$, as compared to a maximum value of 25% for the spontaneous regime. It could be even higher because, in the stimulation regime, time-integrated PL signals contain not only the stimulated emission but also the spontaneous emission. The interference contrast in the stimulation regime decays slowly with increasing $\Delta k_{\|}$ but remains in any case significantly higher than for the spontaneous regime. The Billet interferometer measurements clearly demonstrate enhanced angular coherence of polaritons above the stimulation threshold, or in other words, transition to a coherent phase state.

In conclusion, we have studied polariton coherence in CdTe microcavity under nonresonant pumping by imaging the far-field emission in the Fourier plane. With increasing pumping power, classical stimulation features, such as thresholdlike behavior, stimulated emission, and spectral narrowing, are observed in the strong exciton-photon coupling regime. We show that the stimulated emission comes from a narrow ring in k space, with a remarkable spatial and angular correlation of the emitting source. These observations demonstrate the spontaneous buildup of a macroscopic and coherent phase out of a reservoir of incoherent polaritons. A better understanding of the condensate formation will require further studies of key parameters, such as temperature, static disorder, or exciton-photon detuning. BEC of polaritons is still an open question since results in this work have been obtained using subpicosecond pumping pulses. Future experiments using cw pumping should clarify the issue of thermal equilibrium of the polariton condensate.

We acknowledge support of this work by the EU Network HPRN-CT-2002-00298 ''Photon-mediated phenomena in semiconductor nanostructures.''

[1] L. Pitaevsky and S. Stringari, *Bose-Einstein Condensation* (Oxford University Press, Oxford, 2003).
[2] M. Anderson, J. Ensher, M. Matthews, C. Wieman, and E. Cornell, Science **269**, 198 (1995).
[3] J. M. Blatt, K. W. Böer, and W. Brandt, Phys. Rev. **126**, 1691 (1962).
[4] D. Hulin, A. Mysyrowicz, and C. B. à la Guillaume, Phys. Rev. Lett. **45**, 1970 (1980).
[5] J. L. Lin and J. P. Wolfe, Phys. Rev. Lett. **71**, 1222 (1993).
[6] Y. E. Lozovik and V. I. Yudson, JETP Lett. **22**, 274 (1975).
[7] D. Snoke, S. Denev, Y. Liu, L. Pfeiffer, and K. West, Nature (London) **418**, 754 (2002).
[8] L. V. Butov, C. W. Lai, A. L. Ivanov, A. C. Gossard, and D. S. Chemla, Nature (London) **417**, 47 (2002).
[9] J. Eisenstein and A. MacDonald, Nature (London) **432**, 691 (2004).
[10] A. Imamoglu, J. R. Ram, S. Pau, and Y. Yamamoto, Phys. Rev. A **53**, 4250 (1996).
[11] D. Porras, C. Ciuti, J. Baumberg, and C. Tejedor, Phys. Rev. B **66**, 85304 (2002).
[12] G. Malpuech, A. Kavokin, A. di Carlo, and J. J. Baumberg, Phys. Rev. B **65**, 153310 (2002).
[13] F. Laussy, G. Malpuech, A. Kavokin, and P. Bigenwald, Phys. Rev. Lett. **93**, 016402 (2004).
[14] L. S. Dang, D. Heger, R. Andre, F. Boeuf, and R. Romestain, Phys. Rev. Lett. **81**, 3920 (1998).
[15] F. Boeuf, R. André, R. Romestain, L. S. Dang, E. Péronne, J. Lampin, D. Hulin, and A. Alexandrou, Phys. Rev. B **62**, R2279 (2000).
[16] H. Deng, G. Weihs, C. Santori, J. Bloch, and Y. Yamamoto, Science **298**, 199 (2002).
[17] R. Stevenson, V. Astratov, M. Skolnick, D. Whittaker, M. Emam-Ismail, A. Tartavskii, P. Savvidis, J. Baumberg, and J. Roberts, Phys. Rev. Lett. **85**, 3680 (2000).
[18] C. Weisbuch, M. Nishioka, A. Ishikawa, and Y. Arakawa, Phys. Rev. Lett. **69**, 3314 (1992).
[19] A. Kavokin and G. Malpuech, *Cavity Polaritons* (Elsevier, Oxford, 2003).
[20] V. Savona, L. Andréani, P. Schwendimann, and A. Quattropani, Solid State Commun. **93**, 733 (1995).
[21] P. G. Savvidis, C. Ciuti, J. Baumberg, D. Whittaker, M. Skolnick, and J. Roberts, Phys. Rev. B **64**, 075311 (2001).
[22] M. Müller, R. André, J. Bleuse, R. Romestain, L. S. Dang, A. Huynh, J. Tignon, P. Roussignol, and C. Delalande, Semicond. Sci. Technol. **18**, S319 (2003).
[23] F. Tassone, C. Piermarocchi, V. Savona, A. Quattropani, and P. Schwendimann, Phys. Rev. B **56**, 7554 (1997).
[24] A. I. Tartakovskii, M. Emam-Ismail, R. M. Stevenson, M. S. Skolnick, V. N. Astratov, D. M. Whittaker, J. J. Baumberg, and J. S. Roberts, Phys. Rev. B **62**, R2283 (2000).
[25] M. Müller, J. Bleuse, and R. André, Phys. Rev. B **62**, 16 886 (2000).
[26] M. Richard, J. Kasprzak, R. André, L. S. Dang, and R. Romestain, J. Phys. Condens. Matter **16**, S3683 (2004).
[27] R. Houdré, C. Weisbuch, R. Stanley, U. Oesterle, and M. Ilegems, Phys. Rev. Lett. **85**, 2793 (2000).
[28] W. Langbein, J. Hvam, and R. Zimmermann, Phys. Rev. Lett. **82**, 1040 (1999).